ELSEVIER

Stability properties of the vertical boundary layers in differentially heated cavities

R. Janssen and S. Armfield*

Water Research Laboratory, Department of Civil Engineering, University of New South Wales, Kensington, Sydney, NSW, Australia

In the present study, the two-dimensional (2-D) stability properties of the vertical boundary layers in a cavity that is differentially heated over two opposing vertical walls is considered. The study is performed by introducing artificial, controlled perturbations at the base of the vertical boundary layer along the hot cavity wall and by following the evolution of these disturbances. For small initial perturbations, the evolution is governed by linear effects. This method accurately predicts the frequency of the bifurcation, which occurs for (much) larger Rayleigh numbers. Convective instability sets in for Rayleigh numbers much smaller than those at which the absolute instability (i.e., the bifurcation) occurs, and these Rayleigh numbers are in reasonable agreement with those for the boundary layer along a plate. The absolute instability does *not* result from the first wave which becomes unstable. For small Prandtl numbers (≤ 2), the unstable waves which lead to the absolute instability are shear-driven, and a single frequency is introduced in the flow after the bifurcation. For larger Prandtl numbers, the unstable waves are buoyancy driven and no single-frequency unsteady flow is observed after the bifurcation.

Keywords: natural convection; cavity; convectively unstable; energy balance

Introduction

A classical configuration in heat transfer research and engineering is the differentially heated cavity in which a natural convection flow is established inside a rectangular enclosure by differentially heating two opposing vertical walls. Apart from its many engineering applications, the flow in this configuration has also been used as a benchmark case to test and validate computer-codes written to solve the Navier–Stokes equations.

Although early investigations were concerned mainly with steady flows, emphasis later shifted towards time-dependent flows. Whereas some of this work considered the *transient* flow immediately after the temperature difference between the vertical cavity walls has been imposed (Patterson and Imberger 1980; Armfield and Patterson 1992), most of the work regarding time-dependent aspects of the cavity flow has been concerned with the transitional instabilities arising (for sufficiently large Rayleigh numbers) in the large-time solution of the Navier–Stokes equations. These instabilities indicate the beginning of the transition from steady, laminar to unsteady, turbulent flow. In the square cavity with adiabatic horizontal walls, filled with moderate Prandtl number fluids ($0.2 \leq Pr \leq 10$), at least two different types of instabilities have been found. One instability occurs for the lower range of Prandtl numbers ($Pr \leq 2$) in the horizontal fluid layers near those corners where the vertical boundary layers are turned horizontal by the adiabatic walls. Originally, this corner instability was, somewhat speculatively, denoted as an internal hydraulic jump (Ivey 1984; Paolucci and Chenoweth 1989). Later research (Patterson and Armfield 1990; Janssen and Henkes 1995) showed that it was not a hydraulic jump with Janssen and Henkes suggesting it was an inflexion-point Kelvin–Helmholtz-type instability. The second instability found in the cavity, arises in the boundary layers along the hot and cold vertical cavity walls. Visualization of the oscillations which result from this instability shows a travelling wave-like appearance of the perturbations in the boundary layers and consequently, this instability has been compared with the instability occurring in a natural convection boundary layer along an isolated, semi-infinite, hot vertical plate (Le Quéré and Alziary de Roquefort 1985, 1986; Janssen and Henkes 1995).

The present study investigates in detail the stability properties and the nature of the disturbance amplification in the vertical boundary layers of the differentially heated cavity. This is accomplished by introducing artificial disturbances at the upstream end of the (hot) vertical boundary layer and by following the growth of these disturbances as suggested by Armfield and Janssen (1996). This approach closely predicts the frequency of the naturally occurring instability in the vertical boundary layers. It is shown that the local critical Rayleigh number, beyond which instabilities are amplified in the boundary layer, is several orders of magnitude less than the Rayleigh number at which the naturally-occurring instability is found and that it is in reasonable agreement with the values predicted by a linear stability analysis for the isolated plate. Furthermore, contrary to the assumption usually made (Le Quéré and Alziary de Roquefort 1985, Janssen

* Present address: Department of Mechanical and Mechatronic Engineering, University of Sydney, Sydney, NSW 2006, Australia

Address reprint requests to R. J. A. Janssen, Unilever Research Laboratorium, Section 3084 (Detergents Processing) Post bus 114, 3130 AC Vlaardingen, The Netherlands

Received 1 June 1995; accepted 18 May 1996

Int. J. Heat and Fluid Flow 17: 547–556, 1996

655 Avenue of the Americas, New York, NY 10010

0142-727X/96/$15.00
PII S0142-727X(96)00077-5

and Henkes 1995), the waves which become unstable first are *not* those which lead to the bifurcation of the boundary layer in the cavity. Also, it is found that there is a shift for increasing Prandtl number from the disturbance growth being shear-driven to buoyancy-driven.

Governing equations

Flow equations

Consider a two-dimensional (2-D) rectangular cavity with height H and width L and with isothermal vertical sidewalls. The left wall is held at a fixed temperature T_h and the right wall at a fixed temperature T_c ($T_h > T_c$). The horizontal top and bottom walls are considered to be perfectly adiabatic. The gravitation g acts in the negative x_2-direction (see Figure 1).

The flow in the rectangular cavity is fully described by the 2-D Navier–Stokes equations. Under the Boussinesq approximation, these equations read:

$$\frac{\partial u_i}{\partial x_i} = 0$$

$$\frac{\partial u_i}{\partial t} + u_j \frac{\partial u_i}{\partial x_j} = -\frac{1}{\rho}\frac{\partial p}{\partial x_i} + g\beta(T - T_0)\delta_{i2} + \nu \frac{\partial^2 u_i}{\partial x_j^2}$$

$$\frac{\partial T}{\partial t} + u_j \frac{\partial T}{\partial x_j} = a \frac{\partial^2 T}{\partial x_j^2} + S' \qquad (1)$$

Here, the summation convention has been used: in every term, a summation has to be performed from 1 to 2 over repeated indices. In Equations (1), u_i denotes the velocity component in the x_i-direction, ρ is the density, p is the pressure, ν is the kinematic viscosity, β is the coefficient of thermal expansion, T is the temperature, T_0 is a reference temperature, and a is the thermal diffusivity. The term S' is not normally part of the Navier–Stokes equations. In the present study, it is used to introduce perturbations in the flow, whose evolution is to be studied. For ease of notation, in the following, u_1 and u_2 are denoted as u and v, respectively, and x_1 and x_2 will be denoted as x and y, respectively.

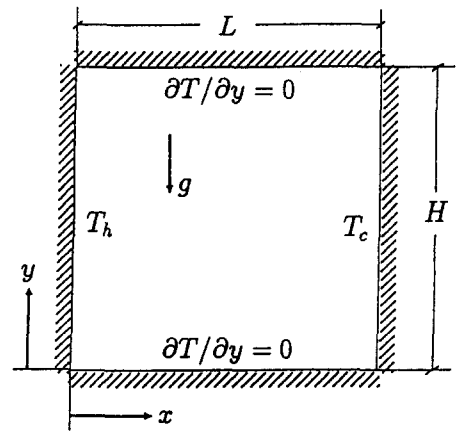

Figure 1 The geometry under consideration

To specify the mathematical problem fully both boundary and initial conditions have to be specified. The boundary conditions used in the present study are:

$$u = v = 0 \qquad x = 0, L \; y = 0, H$$

$$T = T_h \qquad x = 0$$

$$T = T_c \qquad x = L$$

$$\frac{\partial T}{\partial y} = 0 \qquad y = 0, H \qquad (2)$$

The boundary conditions and the geometry suggest a number of scales with which to make the equations dimensionless. Obvious and appropriate choices are the length scale H, the temperature scale $T_0 = T_c$ and the temperature difference $\Delta T = T_h - T_c$. The boundary conditions do not suggest a velocity scale; a possible choice from the parameters in the equations and the boundary conditions is the buoyant scale $(g\beta\Delta T H)^{1/2}$. These choices lead to a set of nondimensionalized equations, governed

Notation

a	thermal diffusivity
A	height over width aspect ratio, $= H/L$
A_{max}	amplitude of imposed perturbation
E_{buoy}	buoyancy production of energy
E_{shear}	shear production of energy
f	frequency
g	acceleration of gravity
H	height of cavity
L	width of cavity
p	pressure
Pr	Prandtl number, $= \nu/a$
Ra	Rayleigh number, $= g\beta\Delta T H^3/(\nu a)$
t	time
S'	source term in temperature equation
T	temperature
T_0	reference temperature
u	horizontal velocity component
u_i	velocity component, $i = 1,2$
v	vertical velocity component
x	coordinate direction between hot and cold walls
x_i	coordinate direction, $i = 1,2$
y	vertical coordinate direction

Greek

β	coefficient of thermal expansion
δ_{ij}	Kronecker-delta
Δ	difference
ν	kinematic viscosity
ρ	density
ϕ	generic variable

Subscripts

cr	critical value
c	quantity related to cold vertical wall
h	quantity related to hot vertical wall

by only three characteristic numbers: the Rayleigh number $\mathrm{Ra} = g\beta\Delta TH^3/(va)$, the Prandtl number $\mathrm{Pr} = v/a$ and the aspect ratio $A = H/L$.

Also the additional source term S' needs to be specified. It is equal to zero everywhere except in a small region at the base of the hot vertical boundary layer: $0 \le x/H \le 0.02$ and $0 \le y/H \le 0.02$. Within this region, three different sources have been employed:

$$S'(t) = A_{\max}\sin(2\pi ft) \tag{3}$$

$$S'(x,t) = A_{\max}\sin\left(2\pi\frac{x/H}{0.02}\right)\sin(2\pi ft) \tag{4}$$

$$S'(t) = 2A_{\max}[\mathrm{ran}(t) - 0.5] \tag{5}$$

Here, $A_{\max}$ denotes the amplitude of the source term and f the frequency of the perturbation. In the third source, Equation 5, the function ran denotes a random source generator with a uniform distribution between 0 and 1.

Kinetic energy equation

Although the Navier–Stokes Equations 1–5 completely describe the mathematical problem, for the present study, it is instructive to consider the kinetic energy, for which the conservation equation can be derived from the Navier–Stokes equations. To derive the equation describing the conservation of *fluctuating* kinetic energy, we first perform the Reynolds decomposition into a mean and a fluctuating quantity. For a scalar variable $\phi(x_i,t)$, this means:

$$\phi(x_i,t) = \bar{\phi}(x_i) + \phi'(x_i,t)$$

$$\text{with } \bar{\phi}(x_i) = \lim_{t^*\to\infty}\frac{1}{t^*}\int_{-t^*/2}^{t^*/2}\phi(x_i,t)\,\mathrm{d}t \tag{6}$$

The equation describing the conservation of fluctuating kinetic energy, $u_i'u_i'/2$, can be derived from the momentum equation in the Navier–Stokes equations. First, the momentum equation is multiplied by u_i after which the decomposition is introduced in the resulting equation. From this equation, the original momentum equation multiplied by $\bar{u}_i$ is subtracted. This results in an equation describing the conservation of fluctuating kinetic energy, which reads:

$$\frac{\partial(u_i'u_i')/2}{\partial t} = \underbrace{-\frac{\partial}{\partial x_j}\left(u_i'\bar{u}_j\bar{u}_i + u_ju_i'u_i'/2 + u_j'p/\rho + \nu u_i'\frac{\partial u_i}{\partial x_j}\right)}_{\mathrm{I}}$$
$$\underbrace{+\bar{u}_i\bar{u}_j\frac{\partial u_i'}{\partial x_j} - \nu\frac{\partial\bar{u}_i}{\partial x_j}\frac{\partial u_i'}{\partial x_j} + g\beta u_i'(\bar{T}-T_0)\delta_{i2}}_{\mathrm{II}}$$
$$\underbrace{+ -u_i'u_j'\frac{\partial\bar{u}_i}{\partial x_j} - \nu\left(\frac{\partial u_i'}{\partial x_j}\right)^2 + g\beta u_i'T'\delta_{i2}}_{\mathrm{III}} \tag{7}$$

Here, the first group of terms on the righthand side (denoted by I) is a divergence, which can be interpreted as representing transport of fluctuating kinetic energy and is zero after integrating over the entire cavity. The second group, denoted by II, contains terms that are all *linear* in the fluctuating velocity components. Reynolds-averaging of Equation 7 would make the terms in this group zero. Group III contains terms which neither by integration in space nor by integration in time can be made equal to zero. These terms describe production and dissipation of fluctuating kinetic energy. The term $-u_i'u_j'\partial\bar{u}_i/\partial x_j$ describes the production of fluctuating kinetic energy by the shear in the mean flow, $g\beta u_i'T'\delta_{i2}$ describes the production of fluctuating kinetic energy by buoyancy forces, and $-\nu(\partial u_i'/\partial x_j)^2$ describes the viscous dissipation of fluctuating kinetic energy.

Numerical method

The equations are discretized using the finite-volume method in which the differential equations are integrated over separate volumes into which the domain is divided. Subsequently, a time-integration is performed using the Crank–Nicholson method. The remaining derivatives are approximated using a second-order–centred finite differences. The convective terms are approximated using the QUICK scheme (Leonard 1979). In the present study, a nonstaggered mesh has been used. To enforce continuity, a Poisson pressure correction equation is used. To avoid the problem of the well-known grid-scale pressure oscillation for a nonstaggered grid, additional elliptic correction terms are incorporated in the continuity equation. These additional terms have been shown to have a negligible effect on the accuracy of the solution (Armfield 1991, 1994).

The grid nodes are distributed using a stretched grid. The basic grid uses 99×99 grid points. These are distributed symmetrically with respect to the cavity half-width and half-height. The first gridpoint is located $0.001H$ in from the walls. Subsequently, the mesh expands at a rate of 7.6% up to $x = 0.1H$, just beyond the edge of the boundary layer. Beyond $x = 0.1H$, the mesh size is constant. Grid refinement is performed by subsequently reducing the distances between the grid points by an integer factor. Because we are interested mainly in the vertical boundary layers in the cavity, grid refinement in the x-direction is performed only within the vertical boundary layers (*i.e.*, for $|x - x_{\mathrm{wall}}| \le 0.1H$); whereas, it occurs everywhere in the y-direction.

Fundamental aspects of the flow

Basic flow structures

Figure 2a shows streamlines for the steady flow of water ($\mathrm{Pr} = 7.5$) in the square cavity at $\mathrm{Ra} = 6 \times 10^8$. The flow in the cavity is clearly dominated by the presence of a large core region in which the velocity is almost horizontal. Along the walls, boundary layers are formed. These boundary layers are especially pronounced along the vertical walls and are similar, but not identical, to those along an isolated, heated or cooled, vertical plate as the results of Henkes and Hoogendoorn (1993) illustrate. They found that characteristic quantities for these boundary layers in the cavity, such as the Nusselt number and the maximum of the vertical velocity component at half the cavity height, adhere to the same scaling with Rayleigh number as do the corresponding quantities for the boundary layer along the isolated plate. A characteristic of the core region in the cavity is its stable stratification, as is clearly evident from Figure 2b, which shows the temperature field in the cavity. This stratification exerts a considerable influence on the boundary layers along the vertical walls of the cavity, as is shown in Figure 2c. This figure shows the profile of the vertical velocity in the boundary layer along the hot wall at half the cavity height. The presence of a region in which the velocity is negative is noticeable. This negative velocity is a direct consequence of the stratification in the interior of the cavity (Henkes and Hoogendoorn).

If the Rayleigh number in the cavity configuration is increased to sufficiently large values, the flow will undergo a number of bifurcations which result in it becoming time dependent and ultimately turbulent. One of these bifurcations causes

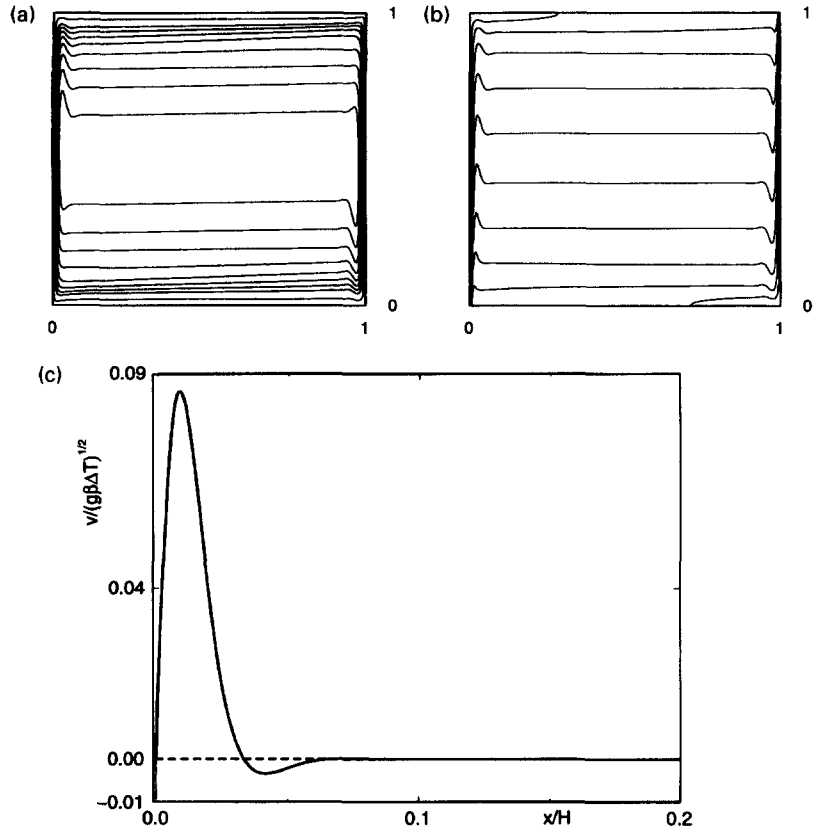

Figure 2 Steady flow in the square cavity; $Ra = 6 \times 10^8$ and $Pr = 7.5$; (a) streamlines, (b) isotherms; (c) profile of the vertical velocity component at half the cavity height

oscillations which are strongest in the downstream parts of the vertical boundary layers (Janssen and Henkes 1995) and for which the visualization (Le Quéré and Alziary de Roquefort 1985) shows that they have a travelling wave-like appearance. This, together with the well-known result that natural-convection boundary layers along isolated heated plates allow wave-like disturbances to develop, suggests that the boundary layers in the cavity behaves in a similar way and that this ultimately leads to a bifurcation of the boundary layer.

Boundary-layer instabilities

Many studies have been performed in which the stability properties of boundary layers are investigated. Attention has been mostly restricted to forced-convection boundary layers (see Drazin and Reid 1981). Probably the simplest way to study the stability properties of boundary layers numerically is by employing linear stability theory and assuming that the boundary layer is a parallel flow. This approach allows the stability problem to be formulated as a generalized eigenvalue equation, known as the Orr–Sommerfeld equation (for forced-convection boundary layers). Solving the *spatial* Orr–Sommerfeld problem, results in the determination of stable and unstable waves with a *fixed* frequency and a particular (normalized) amplitude distribution across the boundary layer and a wavenumber which depend on this frequency. Usually, waves are sought which are neutrally stable (i.e., neither decay nor grow) and it is then generally *assumed* that the mode which becomes unstable first (i.e., for the smallest Rayleigh number) dominates the final disturbance. An important characteristic of these calculations is that all quantities have the same growth rate.

Linear stability studies using an eigenvalue approach have also been performed for natural-convection boundary layers along a vertical plate. Gill and Davey (1969) determined the stability characteristics of the one-dimensional (1-D) natural-convection boundary layer in an environment that was stably stratified similar to the core region in the cavity (Figure 2b). In their analysis, however, the temperature of the plate also increases with height, contrary to the situation in the cavity. To obtain additional results for the boundary layer, eigenvalue calculations were performed in the present study using as a base flow the similarity solution of the natural-convection boundary layer along a hot, isothermal plate in an isothermal environment. The stability equations were discretized using a pseudospectral method employing Chebyshev polynomials, and the resulting generalized eigenvalue equation was solved. The neutral stability results for the most unstable waves (i.e., the waves with the smallest critical Rayleigh number) for both configurations are given in Table 1 for the Prandtl numbers concerned. The frequencies in Table 1 have been made dimensionless with the time scale $\nu^{1/3}(g\beta\Delta T)^{-2/3}$, following the suggestion of Gebhart and Mahajan (1975). This time scale has been chosen because it does not contain the position along the plate, and it is, therefore, a natural time scale for the boundary layer. Here, $\Delta T = 2(T_h - T_\infty)$, where T_h is the temperature of the plate and T_∞ the temperature at infinity. The factor 2 is introduced to make a meaningful comparison with the results for the cavity possible [$2(T_h - T_c)$ corresponding to $T_h - T_c$]. Note, however that $(Ra_y)_{cr}$ is still based on $(T_h - T_\infty)$.

A fundamental assumption in this type of analysis is that of a parallel base flow on which the disturbances develop. This as-

Table 1 Neutral stability results for the critical waves in a natural-convection boundary layer using an eigenvalue analysis

Pr	Isothermal environment (present study)		Stratified environment (Gill and Davey 1969)	
	$\frac{f\nu^{1/3}}{(g\beta\Delta T)^{2/3}}$	$(Ra_y)_{cr}$	$\frac{f\nu^{1/3}}{(g\beta\Delta T)^{2/3}}$	$(Ra_y)_{cr}$
0.71	0.0188	1.8×10^5	0.0239	1.1×10^8
2.0	0.0179	1.4×10^5	0.0240	3.6×10^7
7.5	0.0194	1.2×10^5	—	—

sumption, for natural-convection boundary layers, is true only if terms of $O(Ra_y^{-1/4})$ are neglected. If the flow is not assumed to be parallel, the situation changes radically (Fasel and Konzelmann 1990; Bertolotti et al. 1992). Growth rates now depend on the quantity observed and the position in the boundary layer. Different definitions of the local growth rate vary $O(Ra_y^{-1/4})$. Consequently, it is impossible to define a unique critical Rayleigh number at which the boundary layer becomes unstable. Either the specific quantity and position on which the growth rate is based must be given or approximate ranges must be indicated in which growth first occurs. Some ambiguity in this latter case is, however, to be expected.

Convective and absolute instabilities

The stability studies for boundary layers, described in the previous section, give conditions under which an *imposed* perturbation is first amplified by the boundary layer. The flow is then unstable in the sense that it acts as an amplifier for externally imposed disturbances. Such a flow is called a *convectively* unstable flow. Consequently, if the external source of the perturbation is removed, the amplitude of the oscillation at any fixed position will decrease to zero for sufficiently large time even though the amplitude of the disturbance increases while it is being convected downstream. This behaviour is fundamentally different from that which occurs when the boundary layer in the cavity bifurcates. In this case, the disturbance in the flow at any fixed position is selfsustaining; i.e., the amplitude does not decrease in time. The flow acts as a true oscillator and is termed *absolutely* unstable. Normally, flows become convectively unstable first and absolutely unstable later (*i.e.*, for larger Rayleigh number in the present case). A detailed and rigorous exposition on the concepts of convective and absolute instability is given in Huerre and Monkewitz (1990) and references therein.

Results

Calculations have been performed for different combinations of Ra, Pr, and A although results here are only presented for the flow in the square cavity ($A = 1$). Three different Prandtl numbers (0.71, 2.0, and 7.5) have been selected which cover the basic range of interest. The corresponding Rayleigh numbers are Ra = 10^8, 10^9, and 6×10^8, respectively. These are chosen to be somewhat below the critical value at which the flow in the cavity undergoes transition from steady to time-dependent flow. For Pr = 0.71 and 2.0, the Rayleigh number is, therefore, restricted by the occurrence of the corner instability (mentioned in the Introduction) which occurs at a lower Rayleigh number than the instability in the vertical boundary layers (see Janssen and Henkes 1995).

Validity of the imposed-perturbation approach

Suitability. For the present results to have a general meaning, it is necessary for the disturbance to correspond to an eigenmode of the boundary layer in the cavity. In this study, the imposed perturbation (usually) has a fixed frequency, but the initial amplitude distribution across the width of the boundary layer will not correspond to that of the eigenmode of the boundary layer with the same frequency. There will, therefore, be an evolution from the imposed distribution of the wave amplitude to the distribution corresponding to the eigenmode, and results in the lower part of the boundary layer along the hot cavity wall will depend on the particular form of the source employed in disturbing the flow. Figures 3a and 3b show the distribution of the perturbation amplitude in the temperature across the hot vertical boundary layer at $y = 0.15H$ and the growth of T'_{max} with respect to y for $y > 0.15H$ using two different sources for Pr = 2, Ra = 10^9 with

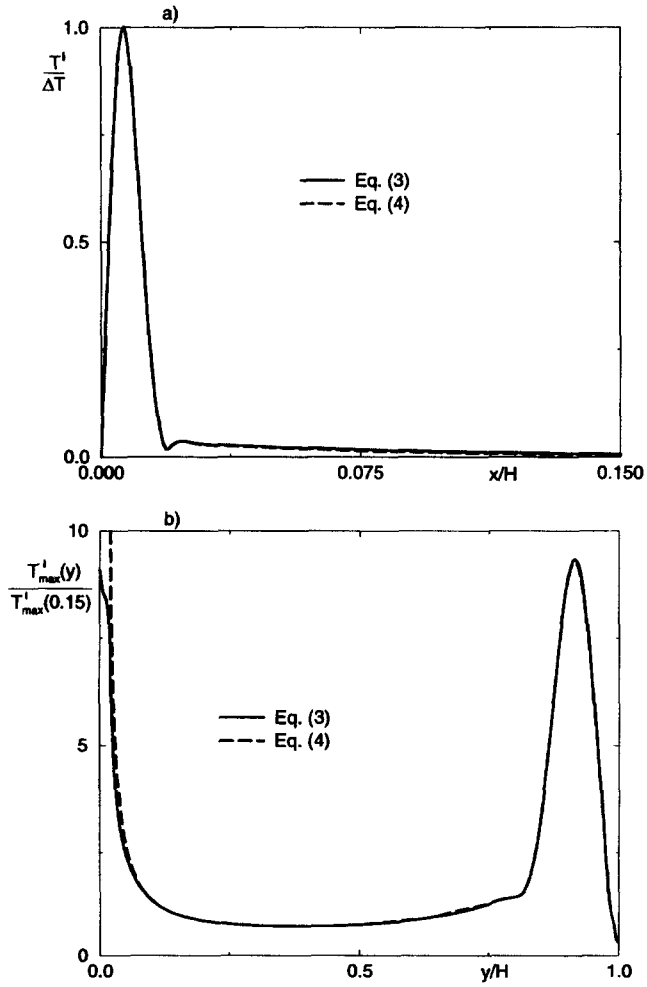

Figure 3 Temperature perturbations in the cavity boundary layer using two different sources: (a) Amplitude across the boundary layer at $y = 0.15H$; (b) T'_{max} as a function of y

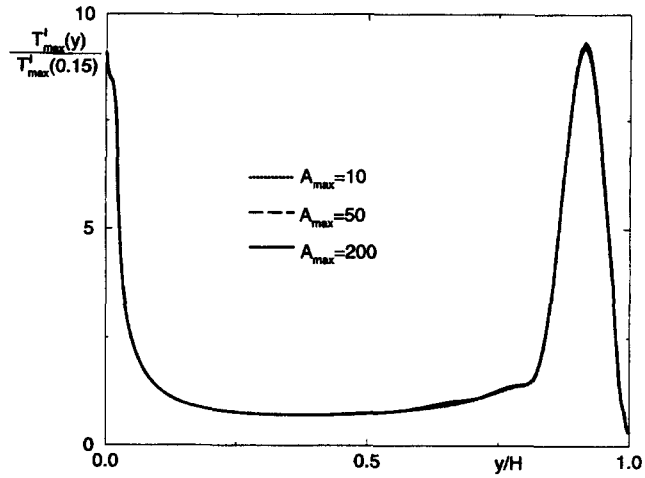

Figure 4 Normalized temperature perturbation growth $T'_{max}(y)/T'_{max}(0.15)$ for various initial source amplitudes

$f\nu^{1/3}(g\beta\Delta T)^{-2/3} = 0.0146$. Here $T'_{max}(y)$ denotes the maximum of the amplitude of the perturbation T' across the width of the boundary layer at height y. The sources used are given in Equations 3 and 4 and differ, therefore, only in the initial distribution of the amplitude across the boundary layer. There is clearly an excellent agreement between the two cases, showing that at least for $y/H \geq 0.15$, the eigenmode for the boundary layer has been selected.

Linearity. Figure 4 shows the growth of T'_{max} for various initial amplitudes A_{max} of the source term (see Equation 3). Again, the situation considered is for Pr = 2, Ra = 10^9 with $f\nu^{1/3}(g\beta\Delta T)^{-2/3} = 0.0146$. Clearly, there is a large range of amplitudes in which the perturbations are *linearly* amplified (i.e., independent of the initial amplitude) by the flow in the boundary layer along the vertical cavity walls.

Accuracy. To investigate the accuracy of the present numerical method, calculations have been performed for different grids. Figure 5 shows the results for the growth of T'_{max} for Pr = 2 and Ra = 10^9. Three different grids have been employed with 99×99, 237×197 and 237×393 grid points. The figure shows that approximately 237×197 grid points are necessary to obtain

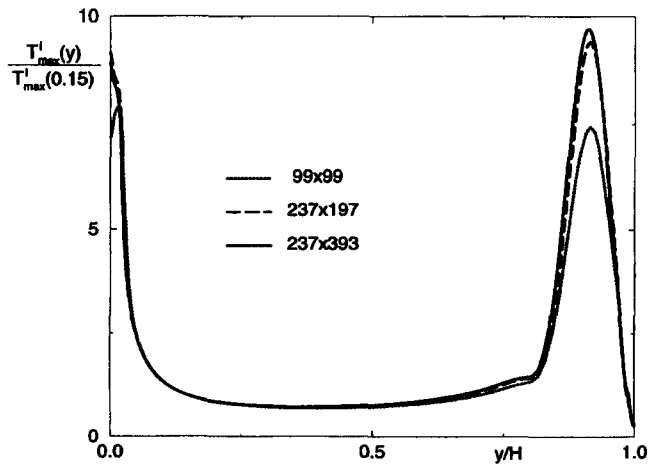

Figure 5 Normalized temperature perturbation growth on different grids

growth rates that are (almost) grid-independent. Furthermore, the results on the coarsest grid, although considerably in error in the region of very large growth rates, clearly have the same trend as the results on the finer grids, showing that the physics is captured even on the coarsest grid. Maximum differences between the integrated growth rates on the two finest grids are approximately 3–4%. For other quantities (e.g., time-averaged quantities), these differences are smaller. Therefore, most calculations have been performed using the grid with 237×197 grid points.

Comparison between plate and cavity

To identify the frequencies of the most unstable waves in the vertical boundary layers of the cavity, calculations were performed using the random source given in Equation 5. Provided the initial amplitude is small enough, the disturbance evolution is described by linearized equations (see preceding section) and, consequently, all the different frequency modes in the random source are decoupled. Spectra were calculated from time series obtained at monitor points located at various height y and at $x = 0.012H$ inside the hot boundary layer. It is assumed that the dominant frequencies at these monitor points are also the dominant frequencies at the same height over the entire width of the boundary layer. The result for Pr = 0.71 at $y = 0.5H$ is shown in Figures 6a and 6b. Figure 6a, in which a logarithmic scale for the power spectral density has been used, shows that only frequencies in a rather narrow range contain energy which differs considerably from the noise level, thereby showing the selective frequency amplification mechanism originally discovered for the vertical plate (Gebhart and Mahajan 1975). Figure 6b shows the same result plotted on a linear scale. Clearly, the most strongly amplified frequency up to $y = 0.5H$ (i.e., the frequency with the strongest *integrated* growth up to this height) corresponds to $f\nu^{1/3}(g\beta\Delta T)^{-2/3} = 0.0340$. This frequency is dominant over the entire range $0.20H \leq y \leq 0.65H$. Figure 7 shows the power spectrum at $y = 0.9H$ with a dominant frequency $f\nu^{1/3}(g\beta\Delta T)^{-2/3} = 0.0223$. This latter frequency is, in fact, in good agreement with the value for the naturally occurring instability which is $0.0230(g\beta\Delta T)^{2/3}\nu^{-1/3}$ (Janssen and Henkes 1995) at Ra = 3×10^8, again, confirming the suitability of the imposed-perturbation approach for analyzing the stability properties of the vertical boundary layers in the cavity.

An obvious observation from the spectra for Pr = 0.71 at $y = 0.5H$ and $y = 0.9H$ is the occurrence of a shift in the most strongly amplified frequency between the two heights in the cavity. This shift, together with the good agreement between the dominant frequency at $y = 0.9H$ and the frequency of the naturally occurring instability clearly shows that the naturally occurring instability in the cavity does *not* correspond to the first mode which becomes unstable. Similar calculations, using a random source to introduce the perturbations in the flow were also performed for the other configurations. For all Prandtl numbers, it was found that there was a similar shift in the dominant frequencies between various heights of the cavity. Basic results are given in Table 2. Because of the observed shift in frequencies, the dominant frequency (i.e., the frequency with the largest integrated growth rate up to that height) is shown for both $y = 0.5H$ and $y = 0.9H$. If these frequencies are compared with the frequencies calculated for the plate as tabulated in Table 1, then it is clear that there is no direct quantitative correspondence. Nevertheless, the similarity between the two configurations is obvious from the closeness of the values of the dominant frequencies of the plate and cavity configurations.

Apart from the frequencies of these dominant waves, also the approximate critical Rayleigh numbers of the waves are given in Table 2. These critical Rayleigh numbers are local Rayleigh numbers; i.e., they are based on the local height y and the local

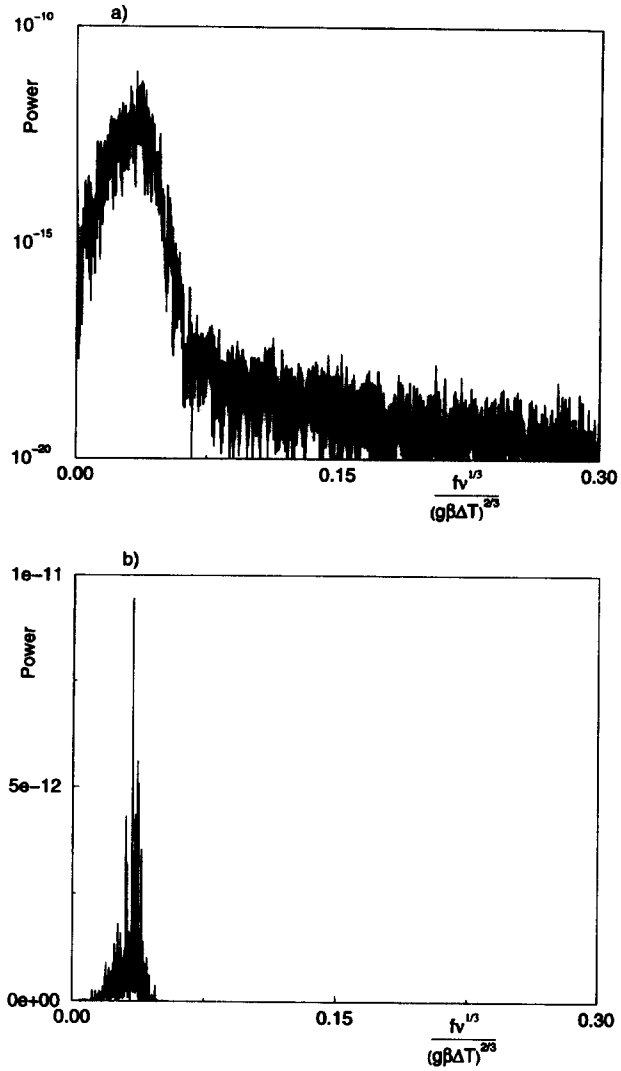

Figure 6 Power spectrum for the temperature in the vertical boundary layer at $(x/H, y/H)=(0.012, 0.75)$ with the random source: (a) logarithmic power scale; (b) linear power scale

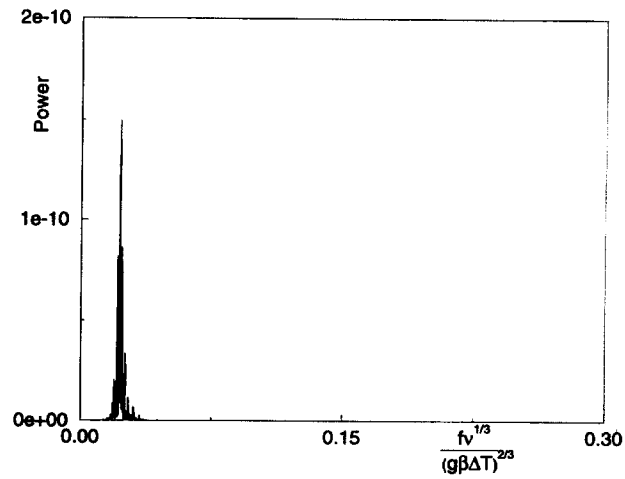

Figure 7 Power spectrum for the temperature in the vertical boundary layer at $(x/H, y/H)=(0.012, 0.9)$ with the random source

temperature difference, at that same height y, between the hot wall and the core region at half the cavity width. The Rayleigh numbers have been estimated by performing new calculations using the single-frequency perturbation as given in Equation 3. Because of the ambiguity in defining growth rates (see the Boundary-layer instabilities section) and because of the resulting ambiguity in finding the critical Rayleigh number, a range is indicated in Table 2. This range is estimated based on growth rates obtained from both T'_{max} and v'_{max}. Here, v'_{max} denotes the maximum of the amplitude of the perturbation v' across the boundary layer. As the results in the table show, the lowest critical Rayleigh numbers are approximately 2×10^5 for the frequencies that are dominant at $y=0.5H$. The highest critical Rayleigh number is observed to be approximately 2×10^7 for $Pr=2$ for the mode that becomes dominant at the extreme downstream end of the vertical boundary layers.

Because cavity flows are different flows for different cavity Rayleigh numbers (i.e., there is no mathematical similarity), it is to be expected that the calculated values for the local critical Rayleigh numbers and frequencies will be different for other cavity Rayleigh numbers. Hence, it was necessary to perform additional calculations to check the magnitude of this influence of the cavity Rayleigh number. Calculations were performed for $Pr=7.5$ for cavity Rayleigh numbers 10^8 and 6×10^7 (as compared to the original calculations for 6×10^8). Calculated local critical Rayleigh numbers for T'_{max} were found to be 4×10^5 and 5×10^5, respectively. Hence, a tenfold increase in the cavity Rayleigh number results only in an approximately twofold decrease in the observed local critical Rayleigh numbers. This, together with the inevitable ambiguity in the determination of the local critical Rayleigh numbers because of the nonparallelism of the cavity boundary layers (an ambiguity which is actually larger than the one introduced by this variation in the cavity Rayleigh number) shows that it is permissible to take the values for the particular configurations considered in Table 2 as representative for the entire range of cavity Rayleigh numbers of interest.

The critical Rayleigh numbers given are those estimated for modes that are dominant (i.e., have a largest *integrated* growth) at $y=0.5H$ and $y=0.9H$. These modes are not necessarily the modes that become unstable first in the cavity. However, checking the results for the calculations with random sources shows that the first amplification for these frequencies starts at approximately the same positions as for the waves given in Table 2. In view of the small differences in the observed critical Rayleigh

Table 2 Results for the most unstable waves in the vertical boundary layers of the cavity at $y=0.5$H and $y=0.9$H

	$y=0.5H$			$y=0.9H$		
Pr	0.71	2.0	7.5	0.71	2.0	7.5
$\frac{fv^{1/3}}{(g\beta\Delta T)^{2/3}}$	0.0340	0.0388	0.0233	0.0223	0.0146	0.0256
$(Ra_y)_{cr}\times10^{-5}$	2–8	1–7	3–4	10–40	100–300	10–15

numbers using this approach and in view of the ambiguity of the definition of the critical Rayleigh number for nonparallel flows, we, therefore, simply take the lowest critical Rayleigh numbers in Table 2 as *the* critical Rayleigh numbers at which the first unstable modes appear. If these values are compared to those of the plate configuration in Table 1, it is clear that there is a reasonable agreement with the values obtained for the boundary layer in an isothermal environment but a poor agreement with those for the boundary layer in a stratified environment. This measure of agreement between the critical Rayleigh numbers for the isolated plate and the cavity configuration also clarifies the previously found discrepancies (see e.g., Le Quéré 1990; Janssen and Henkes 1995). In the earlier investigations, the critical Rayleigh numbers for the *convective* instability in the boundary layer along the plate was compared to that of the *absolute* instability in the cavity. This results in large discrepancies; whereas, the present calculations show conclusively that there is, in fact, a convectively unstable region in the cavity boundary layers for local Rayleigh numbers of the order of those for the isolated plate.

Instability mechanisms

Janssen and Henkes (1995) found, after an extensive set of calculations, that there was for $\mathrm{Pr} \geq 2.5$ an immediate transition from the steady to a time-dependent flow regime with continuous (i.e., broadband) power spectra. This was in marked contrast to the results for $\mathrm{Pr} \leq 2$ for which the bifurcation in the vertical boundary layers of the cavity introduces a *single* frequency in the flow. Janssen and Henkes (1995), therefore, concluded that there was a change in the nature of the instability occurring in the vertical boundary layers when the Prandtl number is increased.

As first described by Nachtsheim (1963), there are—at the least—two possible mechanisms which may be responsible for the amplification of perturbations in a natural-convection flow. This can be seen mathematically from the terms in group III of Equation 7, which describe the production and dissipation of fluctuating kinetic energy of the perturbation. The first term of group III describes production of fluctuating kinetic energy by shear of the mean flow; whereas, the third term in group III describes the production of fluctuating kinetic energy by buoyancy. Gill and Davey (1969) found for the critical waves along the plate in a stratified environment that with increasing Prandtl number, the shear-driven mechanism becomes progressively weaker and the buoyancy-driven mechanism more important.

To the best of our knowledge, there is as yet little understanding of the precise physical mechanisms responsible for the observed wave amplification in boundary layers. As far as the shear-driven mechanism is concerned, it is known that viscosity plays an important and rather subtle role in this, because it is found that the solution of the linearized, parallel stability equations is more *un*stable if viscosity is included as compared to when it is excluded (Schlichting 1968). This apparent role of diffusive effects in causing the instability to occur is presumably also the reason for the role of the Prandtl number as observed by Gill and Davey (1969). For increasing Prandtl number, the relative influence of viscosity and thermal diffusivity changes, thereby causing a change in the driving mechanism for the disturbance amplification.

In view of the observed change in the nature of the boundary-layer instability in the differentially heated cavity (see Janssen and Henkes 1995) for the same range of Prandtl numbers as studied by Gill and Davey (1969), it appears likely that this change is related to an increased influence of the buoyancy-driven instability mode. To study this point more closely, the equation describing the conservation of fluctuating kinetic energy, Equation 7, was evaluated for all cases given in Table 2. In all instances, the total production of fluctuating kinetic energy and the respective contributions from the shear- and buoyancy-production terms were calculated for the boundary layer along the hot wall. The region with $x < 0.1H$ and $y > 0.02H$ was considered ($y > 0.02H$ was taken to ensure that the region in which the additional sources are introduced was not considered, see Equation 5). The results for the frequencies that are dominant at $y = 0.9H$ are given in Table 3. As is readily apparent from Table 3, there is, indeed, a shift from the instability being totally shear-driven ($\mathrm{Pr} = 0.71$), to it being dominantly shear-driven with, however, a significant contribution of the buoyancy-production term ($\mathrm{Pr} = 2$) to an instability which is totally buoyancy-driven ($\mathrm{Pr} = 7.5$). Because the results of Janssen and Henkes (1995) indicate that there isn't a single frequency in the flow for $\mathrm{Pr} = 7.5$ after the bifurcation but a range of frequencies, this same calculation was repeated for all frequencies in the range between $0.0226(g\beta\Delta T)^{2/3}\nu^{-1/3}$ and $0.0312(g\beta\Delta T)^{2/3}\nu^{-1/3}$ with a step of $0.00215(g\beta\Delta T)^{2/3}\nu^{-1/3}$. In all instances, the buoyancy-production was dominant. Because the instability modes (given in Table 3) are the ones which, for somewhat larger Rayleigh numbers, result in the bifurcation of the boundary layer in the differentially heated cavity, it is reasonable to extrapolate this result to the naturally occurring instability and, hence, to assume that the shear-driven instability results in a stronger frequency-filtering effect and consequently in a single frequency in the flow after the bifurcation.

Table 3 Energy-contribution of the shear- and buoyancy-production terms to the total production of fluctuating kinetic energy; E_{shear} and E_{buoy} denote shear- and buoyancy-production, respectively

Pr	E_{shear} (%)	E_{buoy} (%)
0.71	97.6	2.4
2.0	71.3	28.7
7.5	−9.3	100

Additional calculations for the frequencies that are dominant at half the cavity height show for $\mathrm{Pr} = 0.71$ and 7.5 the same trends as in Table 3: for $\mathrm{Pr} = 0.71$, the shear-driven mechanism and for $\mathrm{Pr} = 7.5$ the buoyancy-driven mechanism is dominant. For these (extreme) Prandtl numbers only one mechanism operates. However, for $\mathrm{Pr} = 2$, the dominant mode at $y = 0.5H$ is predominantly buoyancy-driven contrary to the result for $y = 0.9H$. This shows (as does in fact the result given in Table 3) that for $\mathrm{Pr} = 2$ both instability mechanisms are active and influence disturbance growth. This, again, confirms that there is a gradual shift in the nature of the instability mechanism with increasing Prandtl number.

Eigenfunctions and critical layers

In the theoretical study of instabilities in boundary layers, an important position is taken by the critical layer, because this is usually the location where the amplitudes are largest. The critical layer is defined as the position where the phase velocity of the eigenmode is equal to the velocity of the base flow. In forced-convection boundary layers, there is only one critical layer, and this constitutes a fundamental difference with natural convection boundary layers for which there are two critical layers: one inside and one outside the position of maximum vertical velocity.

Figure 8 shows the amplitude distributions of v' and T' at $y = 0.75H$ for $\mathrm{Pr} = 0.71$, $\mathrm{Ra} = 10^8$ and $f\nu^{1/3}(g\beta\Delta T)^{-2/3} = 0.0223$. Also shown in the figure is the profile of the steady, vertical velocity component v. The most outstanding feature of these profiles is the presence of three local maxima in the amplitude distribution for v', the inner one of which is located

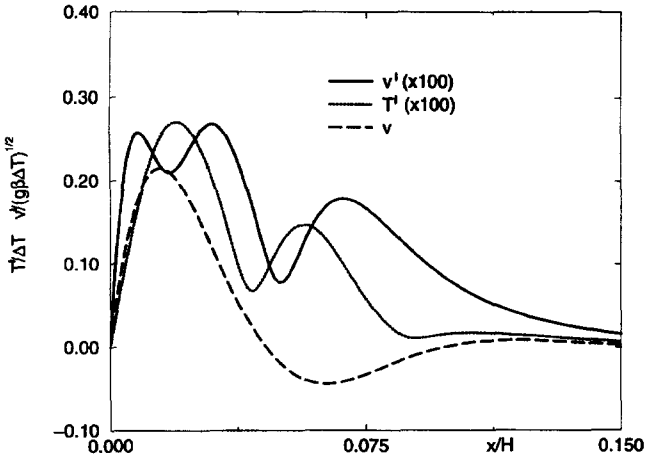

Figure 8 Amplitude distributions of the T'- and v'-perturbations in the vertical boundary layer at $y=0.75$H for Pr$=0.71$; for comparison, also the steady v-velocity profiles is included

between the wall and the position of maximum vertical velocity. In Figure 8, the outer maximum is larger than the inner maximum. This is true for all $y \leq 0.8H$. In fact, for $y \leq 0.6H$, there is no inner maximum in the v'-amplitude (because the amplification is very weak for these heights). However, for $y > 0.8H$ the inner maximum becomes the largest one. The presence of this inner maximum in the v'-amplitude is the main difference between the results for Pr $= 0.71$ and for Pr $= 7.5$, as Figure 9 shows, in which the same results for Pr $= 7.5$ are depicted as in Figure 8 for Pr $= 0.71$. No inner maximum of the v'-amplitude was found for Pr $= 7.5$ at any height. In view of the difference in the energy sources for the modes at the various Prandtl numbers, it is clear that the difference in the amplitude profiles is related to the instability being either shear- or buoyancy-driven. This is confirmed by the results for the two different unstable modes at Pr $= 2$: the dominantly shear-driven mode had an inner maximum in v'; whereas, the buoyancy-driven mode did not.

Similar distributions for the amplitudes of the v'-perturbation (i.e., with an inner maximum for Pr ≈ 0.7 and without it for Pr ≈ 7) were found by Knowles and Gebhart (1968), Gill. and Davey (1969), and Jaluria and Gebhart (1974) in their eigenvalue stability studies for natural convection boundary layers along a plate under various conditions (isothermal and constant-flux walls, stratified and isothermal environments). In all these investigations, the results were for *neutral* waves only. It seems reasonable, however, to extrapolate these results to unstable waves (in fact, we checked this to be the case for the boundary layer along the plate in an isothermal environment using our eigenvalue code). The overall agreement between the results for the plate (under the various conditions studied) and the cavity shows the general applicability of the physics of the instability mechanisms as determined here.

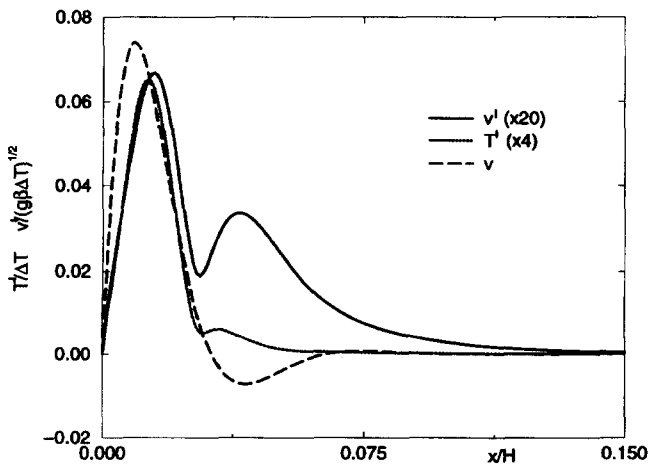

Figure 9 Same as in Figure 8 but for Pr$=7.5$

Conclusions

The present study investigates the stability properties of the vertical boundary layers of a cavity that is differentially heated over two opposing vertical walls. The horizontal walls are adiabatic. The stability properties were determined by introducing controlled perturbations at the base of the hot boundary layer. These perturbations developed into travelling waves which are either amplified or damped when travelling along the boundary layer. Perturbation sources with a monoperiodic and with a random time-dependence have been used.

There are two important advantages of the present approach compared to simply solving the Navier–Stokes equations for successively larger Rayleigh numbers and studying the naturally occurring bifurcation of the vertical boundary layers (as was previously done for this configuration; see e.g., Le Quéré and Alziary de Roquefort 1985; Paolucci and Chenoweth 1989; Janssen and Henkes 1995). Firstly, by perturbing a steady base flow the, in this case undesired, influence of the corner instability (Janssen and Henkes) is avoided, making it possible to investigate the stability properties of the boundary layers in the cavity more directly. Secondly, it is possible in the present approach to calculate convectively unstable waves and to determine their properties. In combination with the previously used method of calculating the naturally occurring bifurcation (i.e., the absolutely unstable waves), the present approach makes it possible to obtain a complete picture of the disturbance growth mechanisms in the boundary layer of the cavity.

It was checked that there was a very rapid development of the unstable waves towards an eigenmode of the vertical boundary layers, indicating the independence of the results with respect to the particular *form* of the particular disturbances that are introduced into the flow. By using sufficiently small initial perturbations, the results didn't depend on the *magnitude* of these initial perturbations. Thus, the present results describe the linear, unstable *eigen*modes of the boundary layer in the cavity.

The present calculations show that the (approximate) critical Rayleigh numbers for the occurrence of convectively unstable modes in the cavity configuration are in reasonable agreement with those for the natural-convection boundary layer along a plate in an isothermal environment. The calculations also show the large difference (approximately 2–3 orders of magnitude) in Rayleigh numbers between the first occurrence of (convectively) unstable modes and the (absolutely unstable) bifurcation. Furthermore, it is clear that the unstable modes which ultimately result in the bifurcation of the boundary layer, are *not* the modes which become unstable first. These results explain why the previously performed comparisons between the cavity and plate configurations (e.g., Le Quéré 1990; Janssen and Henkes 1995) gave large discrepancies. Previously, the *absolute* instability in the cavity was compared to the *convective* instability along the plate. Comparing the convectively unstable region in the cavity to the plate, results in a much better agreement.

An important difference between the present results for the smaller Pr-number values (0.71 and 2) and the larger Pr-value (7.5) is in the energy source for the unstable waves. For Pr ≤ 2, the unstable wave which ultimately leads to the bifurcation of the boundary layer in the cavity, is predominantly *shear*-driven;

whereas, for Pr = 7.5, it is *buoyancy*-driven. Because the results previously obtained for the naturally occurring bifurcation in the cavity flow (Janssen and Henkes 1995) show a monoperiodic oscillation in the flow after the bifurcation for the smaller Prandtl numbers and a broadband power spectrum for the larger Prandtl numbers, the present study suggests strongly that this difference is caused by the change in the energy source for the unstable waves.

Although a quantitative comparison between the plate and the steady-state cavity flow shows the results to be not identical, the agreement in the qualitative appearances of the amplitude distributions for the boundary layer in the differentially heated cavity with those found for neutral modes along the isolated plate (Knowles and Gebhart 1968; Gill and Davey 1969; Jaluria and Gebhart 1974) together with the shift in the main energy source for increasing Prandtl number in both configurations shows the close physical similarity between the configurations. It also shows that the physics of the unstable waves as presented in this paper are of a quite general nature.

References

Armfield, S. W. 1991. Finite difference solutions of the Navier–Stokes equations on staggered and nonstaggered grids. *Computer Fluids*, **20**, 1–17

Armfield, S. W. 1994. Ellipticity, accuracy, and convergence of the discrete Navier–Stokes equations. *J. Comp. Phys.*, **114**, 176–184

Armfield, S. W. and Janssen, R. J. A. 1995. Direct stability analysis of steady state cavity convection flow. *Int. J. Heat Fluid Flow* in press

Armfield, S. W. and Patterson, J. C. 1992. Wave properties of natural-convection boundary layers. *J. Fluid Mech.*, **239**, 195–211

Bertolotti, F. P., Herbert, Th. and Spalart, P. R. 1992. Linear and nonlinear stability of the Blasius boundary layer. *J. Fluid Mech.*, **242**, 441–474

Drazin, P. G. and Reid, W. H. 1981. *Hydrodynamic Stability*. Cambridge University Press, Cambridge, UK

Fasel, H. and Konzelmann, U. 1990. Non-parallel stability of a flat-plate boundary layer using the complete Navier–Stokes equations. *J. Fluid Mech.*, **221**, 311–347

Gebhart, B. and Mahajan, R. L. 1975. Characteristic disturbance frequency in vertical natural convection flow. *Int. J. Heat Mass Transfer*, **18**, 1143–1148

Gill, A. E. and Davey, A. 1969. Instabilities of a buoyancy-driven system. *J. Fluid Mech.*, **35**, 775–798

Henkes, R. A. W. M. and Hoogendoorn, C. J. 1993. Scaling of the laminar natural-convection flow in a heated square cavity. *Int. J. Heat Mass Transfer*, **36**, 2913–2925

Huerre, P. and Monkewitz, P. A. 1990. Local and global instabilities in spatially developing flows. *Ann. Rev. Fluid Mech.*, **22**, 473–537

Ivey, G. N. 1984. Experiments on transient natural convection in a cavity. *J. Fluid Mech.*, **144**, 389–401

Jaluria, Y. and Gebhart, B. 1974. On transition mechanisms in vertical natural convection flow. *J. Fluid Mech.*, **66**, 309–337

Janssen, R. J. A. and Henkes, R. A. W. M. 1995. Influence of Prandtl number on instability mechanisms and transition in a differentially heated square cavity. *J. Fluid Mech.*, **290**, 319–344

Knowles, C. P. and Gebhart, B. 1968. The stability of the natural convection boundary layer. *J. Fluid Mech.*, **34**, 657–686

Leonard, B. P. 1979. A stable and accurate convective modelling procedure based on quadratic upstream interpolation. *Comp. Meth. Appl. Eng.*, **19**, 59–98

Le Quéré, P. 1990. Transition to unsteady natural-convection in a tall water-filled cavity. *Phys. Fluids*, **A2**, 503–515

Le Quéré, P. and Alziary de Roquefort, T. 1985. Transition to unsteady natural convection of air in differentially heated cavities. *Proc. 4th Int. Conference Num. Meth. in Laminar and Turbulent Flow*, 841–852

Le Quéré, P. and Alziary de Roquefort, T. 1986. Transition to unsteady natural convection of air in vertical differentially heated cavities: Influence of thermal boundary conditions on the horizontal walls. *Proc. 8th Int. Heat Transfer Conference*, 1533–1538

Nachtsheim, P. R. 1963. Stability of free-convection boundary-layer flows. NASA TN D-2089

Paolucci, S. and Chenoweth, D. R. 1989. Transition to chaos in a differentially heated vertical cavity. *J. Fluid Mech.*, **215**, 229–262

Patterson, J. C. and Armfield, S. W. 1990. Transient features of natural convection in a cavity. *J. Fluid Mech.*, **219**, 469–498

Patterson, J. C. and Imberger, J. 1980. Unsteady natural convection in a rectangular cavity. *J. Fluid Mech.*, **100**, 65–86

Schlichting H. 1968. *Boundary Layer Theory*. McGraw-Hill, New York, p. 462